Dental Materials Journal 2022; 41(6): 882–888

Fabrication of bioresorbable hydroxyapatite bone grafts through the setting reaction of calcium phosphate cement

Hikaru TAKEYAMA[1,2], Michito MARUTA[1], Taira SATO[3], Noboru KAJIMOTO[1], Eiji FUJII[4], Takashi MATSUURA[2] and Kanji TSURU[1]

[1] *Section of Bioengineering, Department of Dental Engineering, Fukuoka Dental College, Fukuoka 814-0193, Japan*
[2] *Section of Fixed Prosthodontics, Department of Oral Rehabilitation, Fukuoka Dental College, Fukuoka 814-0193, Japan*
[3] *Section of Biomaterials, Department of Dental Engineering, Fukuoka Dental College, Fukuoka 814-0193, Japan*
[4] *Industrial Technology Center of Okayama Prefecture, Okayama 701-1296, Japan*
Corresponding author, Michito MARUTA; E-mail: maruta@college.fdcnet.ac.jp

We prepared hydroxyapatite (HAp) bone grafts by the setting reaction of calcium phosphate cement, and investigated the effects of the porosity and crystallinity on the osteoconductivity and bioresorbability. We examined the effect of the water-mixing ratio, pressure, and post-heat treatment temperature during preparation on the crystallite size and porosity of the HAp blocks. The quantity of protein adsorption increased with increasing porosity and specific surface area (SSA) of the HAp blocks, whereas the initial cell attachment was similar despite the different porosities and crystallinities. In *in vitro* dissolution tests with a pH 5.5 buffer, which mimics an osteoclast-created Howship's lacuna, both the porosity and SSA of the HAp blocks affected the solubility; most likely due to the increased contact area with the buffer. Thus, HAp blocks prepared by the setting reaction of calcium phosphate cement could be applicable for bioresorbable HAp bone grafts because of the high porosity and SSA.

Keywords: Hydroxyapatite, Bioresorption, Osteoconductivity, Bone graft, Howship's lacuna

INTRODUCTION

Hydroxyapatite (HAp) bone grafts have been clinically applied for many years in the fields of orthopedics and oral surgery as nonbioresorbable artificial bone grafts with excellent osteoconductivity[1,2]. Many reports have investigated the introduction of pores into HAp bone grafts[3-12]; most clinically used HAp bone grafts are characterized by their pore structure. Most of these reports focus on micro- to macro-sized pores, especially interconnecting pore structures, which are expected to fuse with surrounding bone tissue through entry into cells and tissues[7-13]. Unfortunately, these pore structures make little contribution to improved bioresorption. On the other hand, because bone tissue is composed of low-crystalline HAp and collagen, research has been conducted on artificial bone grafts by compositing HAp and collagen[14-20]. Recently, a HAp and collagen composite known as ReFIt has been commercialized and used clinically in Japan[19,20]. This new bone graft is bioresorbable and can be replaced by new bone in accordance with bone remodeling. In the future development of artificial bone grafts, not only osteoconductivity but also bioresorption followed by replacement by new bone will be in great demand. Therefore, HAp bone grafts by itself must be studied not only for their osteoconductivity but also for their bioresorption. However, typical HAp bone grafts prepared by sintering are highly crystalline and have a low porosity, which results in poor bioresorption.

For fabricating HAp bone grafts with controllable porosity and crystallinity, we focused on a calcium phosphate cement invented by Brown and Chow[21]. The cement sets at room temperature while undergoing phase transformation to HAp, resulting in a set body with low crystallinity and high porosity. We thought that if a pure HAp single-phase cement set body could be prepared, post-heat treatment could be applied to it to obtain a HAp bone grafts with some degree of crystallinity and porosity control.

In this study, we examined a preparation condition of cement set body with pure HAp single-phase followed by fabrication of HAp blocks with almost the same crystallite size but different porosities, and HAp blocks with almost the same porosity but different crystallinities, by modulating the water-mixing ratio, pressure, and post-heat treatment temperature during preparation through the setting reaction of calcium phosphate cement. Then, we investigated the effects of the porosity and crystallinity on the osteoconductivity and bioresorbability. We used osteoblast-like cells to evaluate the *in vitro* osteoconductivity and *in vitro* dissolution tests in an acidic buffer at pH 5.5, mimicking the resorption environment by osteoclasts, to evaluate the *in vitro* bioresorbability.

MATERIALS AND METHODS

Preparation of powders

Tetracalcium phosphate [TTCP; $Ca_4(PO_4)_2O$] powder as cement raw material was prepared using calcium monohydrogen phosphate (DCPA; $CaHPO_4$, Taihei Chemical, Osaka, Japan) and calcium carbonate ($CaCO_3$, Fujifilm Wako Pure Chemical, Osaka, Japan). A mixture of equimolar mixed powder of DCPA and $CaCO_3$ with isopropyl alcohol (Fujifilm Wako) was placed in a ball mill with zirconia beads (φ 1 mm) and pulverized at 400 rpm

Received Feb 25, 2022: Accepted Jun 16, 2022
doi:10.4012/dmj.2022-045 JOI JST.JSTAGE/dmj/2022-045

for 6 h. After drying at 80°C in a drying oven (SDN27, Sansyo, Tokyo, Japan) for 12 h, the mixture powder was placed in a Pt crucible and heated in an electronic furnace (RHF1600, Carbolite Gero, Hope, England) at a rate of 10°C/min up to 1,500°C, and maintained for 1 h followed by air-cooling to room temperature. The resultant powder with isopropyl alcohol was placed in the ball mill with zirconia beads (φ 1 mm) again and pulverized at 400 rpm for 24 h. DCPA powder as cement raw material was prepared by pulverization of raw DCPA powder. The DCPA raw powder was placed in the ball mill with zirconia beads (φ 1 mm) and isopropyl alcohol and pulverized at 400 rpm for 12 h. The obtained powders were stored in a drying oven at 80°C until use. For these series of powder mills, 30 g of zirconia beads were used for every 10 g of powder. HAp powders (HAp-100 and HAp-200: Taihei Chemical) without any pretreatment were used for further sample preparation.

Preparation of HAp blocks

TTCP and DCPA were weighed to obtain a Ca/P mole ratio of 1.67 and then mixed in a mortar and pestle for 10 min. Deionized (DI) water was produced with DI water production equipment (Elix Essential UV 3, Merck, Darmstadt, Germany). Cement paste was prepared by mixing 1.0 g of the TTCP–DCPA mixed powders with nitrogen-gas-bubbled DI water at a powder-to-liquid (P/L) mass-to-volume ratio of 1.33, 1.67, and 3.33. The pastes prepared at a P/L of 1.33 and 1.67 were placed in a Teflon mold (9-mm diameter and 2-mm thickness), and both sides of each mold were covered with glass plates. The paste prepared at a P/L of 3.33 was placed in a stainless-steel mold (φ9 mm) and pressed uniaxially at either 100 MPa or 150 MPa with a hydraulic press (MT-50HD, NPa System, Saitama, Japan). Then, all the aforementioned pastes were placed in an oven (EO-450V, As One, Osaka, Japan) and maintained at 37°C under 100% relative humidity for 6 h followed by post-treatment at 80°C under 100% relative humidity for 72 h. The resultant blocks (except for one prepared at a P/L ratio of 3.33 and a pressure at 150 MPa) were set in a muffle furnace (HPM-1N, As One), subsequently heated at a rate of 10°C/min up to 850°C, and then maintained for 12 h to obtain HAp blocks. The HAp blocks prepared at P/L ratios of 1.33, 1.67, and 3.33 are denoted as HAp68, HAp55, and HAp42, respectively. The HAp block prepared at a P/L ratio of 3.33 and a pressure at 150 MPa but no post heat-treatment is denoted as HAp42_L. HAp powders (HAp-100, Taihei Chemical), 0.2 g, were placed in a stainless-steel mold (φ9 mm) and pressed uniaxially at 10 MPa, followed by heating at a rate of 10°C/min up to 1,000°C and maintained for 5 h. After cooling to room temperature, the obtained HAp block is denoted as HAp42_H. A typical sintered HAp block was also prepared for comparison. HAp powders (HAp-200, Taihei Chemical), 0.2 g, were placed in a stainless-steel mold (φ9 mm) and pressed uniaxially at 100 MPa, followed by heating at a rate of 5°C/min up to 1,200°C and maintained for 6 h. The obtained HAp block is denoted as sintered HAp. Table 1 shows the sample codes and preparation conditions of HAp blocks.

Characterization of HAp blocks

Compositional analysis of the obtained blocks was performed by X-ray diffraction (XRD; MiniFlexII, Rigaku, Tokyo, Japan). The XRD instrument was set at 30 kV and 15 mA with Cu-Kα radiation, and scanned over the range between 10° and 60° in 2θ at a scanning rate of 2°/min. The line broadening of the (002) and (300) diffraction peaks was used to evaluate the length of the crystallite size along the c-axis and a-axis in accordance with the Scherrer equation, where PDXL software (ver1.8.1; Rigaku) attached to the XRD instrument was used for calibration of the peak full width at half maximum and instrumental broadening.

The porosity was calculated using the following equation [1]:

$$\text{Porosity } (\%)=(1-d_{\text{sample}}/d_{\text{HAp}})\times 100 \quad [1]$$

where d_{sample} is the bulk density of the sample calculated using the weight and external volume of the obtained HAp blocks, and d_{HAp} is the theoretical density of HAp (3.16 g/cm^3)[22]. Seven blocks were used for each HAp block sample to calculate the mean and standard deviation (SD).

The specific surface area (SSA) of the obtained blocks was measured by the Brunauer–Emmett–Teller N_2 adsorption method (Belsorp max, MicrotracBEL, Osaka, Japan).

Table 1 Sample codes and preparation condition of HAp blocks

Sample code	P/L (g/mL)	Pressure (MPa)	Temperature (°C)
HAp68	1.33	b	850
HAp55	1.67	b	850
HAp42	3.33	100	850
HAp42_L	3.33	150	c
HAp42_H	a	10	1,000
Sintered HAp	a	100	1,200

a: conventional pressing and sintering method, b: no pressure load, c: no post heat treatment

Split cross-sections of the obtained blocks were observed by scanning electron microscopy (SEM; JCM-6000 Plus, JEOL, Tokyo, Japan) at an accelerating voltage of 15 kV. For the SEM observations, the split cross-sectioned HAp block was fixed to a holder with Ag dotite (D-550, Nisshin-EM, Tokyo, Japan) and then an electroconductive Au coating was applied onto the HAp blocks with a magnetron sputtering device (DII-29010SCTR Smart Coater, JEOL).

Protein adsorption and initial cell attachment of HAp blocks

As a sterilization process, HAp blocks were immersed in 70% ethanol overnight and then dried in a clean bench. The sterilized HAp blocks were immersed in 300 μL of alpha modified Eagle minimum essential medium (αMEM; Nacalai Tesque, Kyoto, Japan) containing 10% fetal bovine serum (FBS; Gibco, Thermo Fisher Scientific, San Jose, CA, USA), and 1% mixture of penicillin and streptomycin (Fujifilm Wako Pure Chemical), in each well of a 48 well-plate. After contact with HAp blocks for 6 h, 50 μL of the medium was extracted from each well and added to a plastic tube. The quantity of protein in the medium was analyzed with a bicinchoninic acid protein assay kit (Thermo Fisher Scientific). The quantity of protein adsorbed onto the HAp blocks was determined by subtracting the quantity of protein in the medium after 6 h of contact with the HAp blocks from the total quantity of protein in the original medium. Six blocks were used for each group to calculate the mean and SD.

A mouse calvarium-derived osteoblast-like cell line, MC3T3-E1 (Riken BioResource Center, Ibaraki, Japan) was used for the evaluation of initial cell attachment. αMEM containing 10% FBS (Gibco), and 1% mixture of penicillin and streptomycin (Fujifilm Wako Pure Chemical) was used for cell culture. HAp blocks were sterilized by the same method followed by the immersion of FBS-free αMEM for 1 h. The HAp blocks were placed on a cell culture dish (Falcon, CORNING, Corning, NY, USA). Then, a 50-μL cell suspension containing 4×10^4 cells was dropped onto each HAp block and cultured in 5% CO_2 at 37°C. After culturing for 6 h, 5 mL of Dulbecco's phosphate-buffered saline (Gibco) was poured into the culture dish to remove unattached cells. The HAp blocks with cells were moved to a 48-well plate and the cell viability was analyzed with a 3-(4,5-dimethylthiazol-2-yl)-2,5-diphenyltetrazolium bromide cell count kit (Nacalai Tesque). A control sample free from HAp blocks was also tested for comparison. Six blocks were used for each group to calculate the mean and SD.

In vitro dissolution rate of HAp blocks

The *in vitro* dissolution rate was evaluated in accordance with JIS T 0330-3 (2012)[23,24]. Each HAp block was immersed in a sodium acetate–acetic acid buffer at pH 5.5, mimicking the resorption environment of osteoclasts. Calcium ion elution from each HAp block to the buffer was monitored with a Ca-ion-selective electrode (Laqua 8203-10C, Horiba, Kyoto, Japan). This test was performed by fixing the buffer volume of 100 mL per HAp block.

Statistical analysis

Statistical analysis was performed with KaleidaGraph (version 4.5.3, Synergy Software, Reading, PA, USA). One-way analysis of variance (ANOVA) tests with post-hoc Tukey–honestly significant difference tests were used. Differences were considered statistically significant at $p<0.05$.

RESULTS

Figure 1 shows XRD patterns of blocks prepared in this study. A range of 20°–40° is shown in the figure because no relevant peaks were observed in the excluded region. We assigned all the diffraction patterns to HAp (hydroxyapatite: PDF#09-0432), although we observed some differences in crystallinity due to the preparation conditions. Table 2 shows the crystallite size, apparent porosity, and SSA of the HAp blocks. By keeping the post-heat treatment temperature constant, changing the water-mixing ratio during preparation, and applying pressure during slurry molding, HAp blocks with almost the same crystallite size but different porosities (HAp68, HAp55, and HAp42) could be fabricated. Furthermore, by changing the pressure applied during preparation and the post-heat treatment temperature, HAp blocks with similar porosity but different crystallinities (HAp42_L,

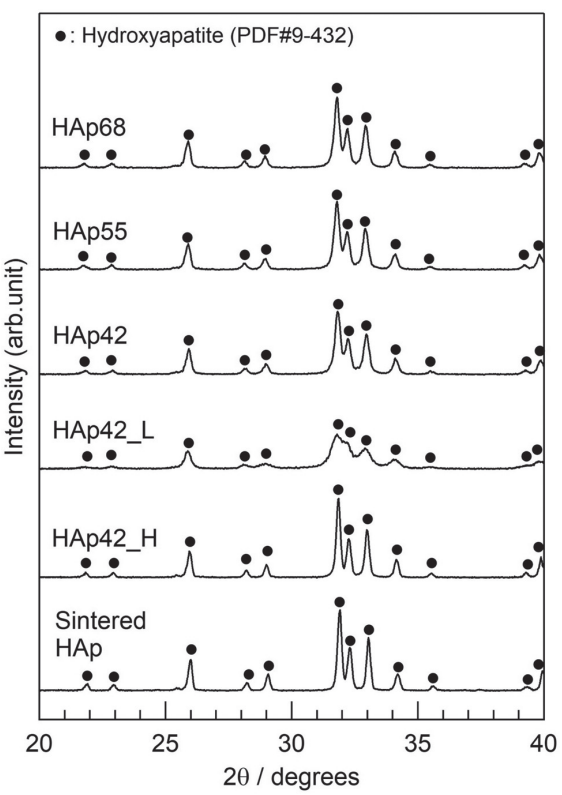

Fig. 1 XRD patterns of HAp blocks.

Table 2 Crystallite size, porosity, and SSA of HAp blocks

Sample code	Crystallite size (nm)		Porosity (%)	SSA (m^2g^{-1})
	002	300		
HAp68	43.1	37.8	68.0±0.4	23.35
HAp55	40.9	37.6	58.2±0.8	19.74
HAp42	42.5	37.8	42.9±0.2	11.00
HAp42_L	31.2	16.1	42.8±0.4	29.93
HAp42_H	49.8	51.0	42.0±0.7	10.86
Sintered HAp	56.0	57.8	5.1±0.6	6.08

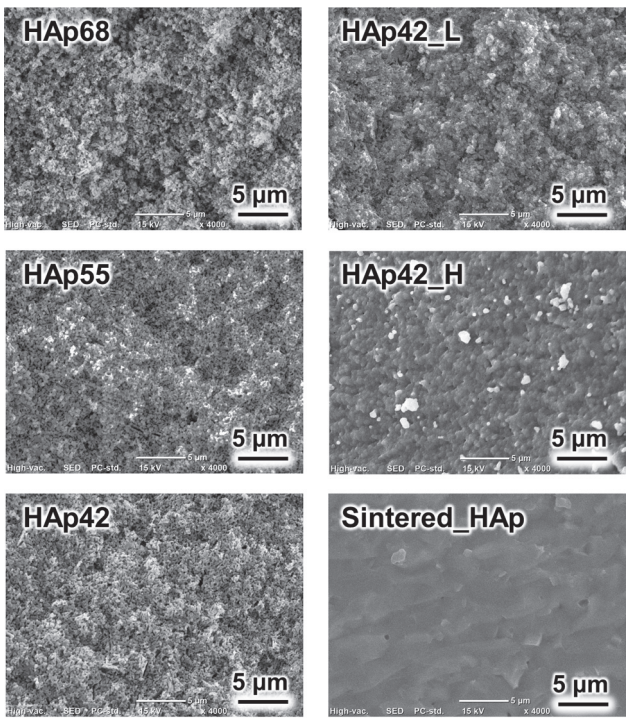

Fig. 2 Cross-sectional SEM images of HAp blocks with different porosities (HAp42, HAp55, HAp68, and HAp75) and crystallite sizes (HAp42, HAp42_L, and HAp42_H), and sintered HAp for comparison.

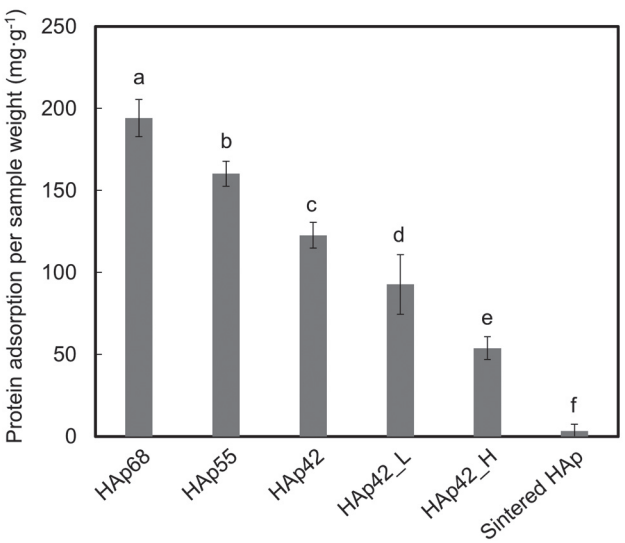

Fig. 3 Quantity of protein adsorbed on HAp blocks after 6 h of immersion in cell culture medium containing 10% FBS.
Different lowercase letters indicate statistically significant differences (p<0.05).

HAp42, and HAp42_H) could be fabricated. The apparent porosity of the sintered HAp block prepared as a comparison was 5.1% and the crystallite size calculated from the diffraction peak (300) was 57.8 nm.

Figure 2 shows cross-sectional SEM images of the HAp blocks. The HAp blocks fabricated through the setting reaction of calcium phosphate cement (HAp68, HAp55, HAp42, and HAp42_L) exhibited numerous pores of nano- to submicron-order in size. These pores were extremely reduced on the surface of HAp blocks produced by the sintering method. We observed some pores in HAp42_H, but almost no pores in sintered HAp, which exhibited a typical surface structure of ceramic materials calcined at high temperature.

Figure 3 shows the quantity of protein adsorbed onto the HAp blocks after immersion in αMEM containing 10% FBS for 6 h. We found statistically significant differences between all the HAp blocks. Comparing the quantity of protein adsorbed by three different porosity samples with constant crystallite size (HAp68, HAp55, and HAp42), the quantity of protein adsorbed increased with increasing porosity (HAp68>HAp55>HAp42). Next, a comparison of the quantity of protein adsorbed by three different crystallite size samples at constant porosity (HAp42_L, HAp42, and HAp42_H) indicated no correlation between the protein adsorption and crystalline size of the HAp block; the quantity of protein adsorption was in the order of HAp42>HAp42_L >HAp42_H whereas the crystalline size was in the order of HAp42_H>HAp42>HAp42_L. The quantity of protein adsorbed onto the sintered HAp was extremely low compared with that of the other HAp blocks.

Figure 4 shows the viability of MC3T3E1 cells

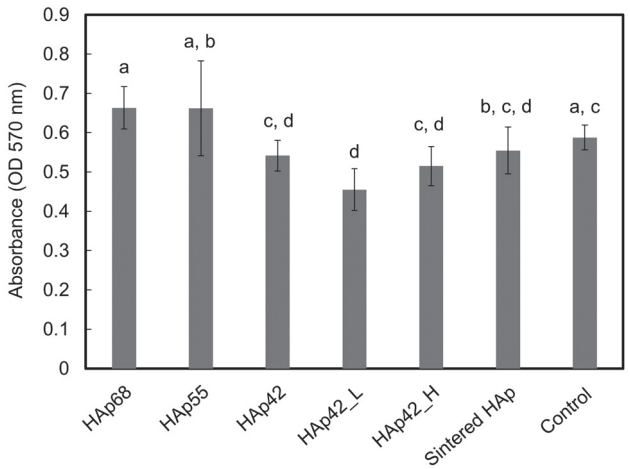

Fig. 4 Viability of MC3T3E1 cells adhered onto HAp blocks after 6 h of culture.
Same lowercase letters indicate no statistically significant differences while different lowercase letters indicate significant differences ($p<0.05$).

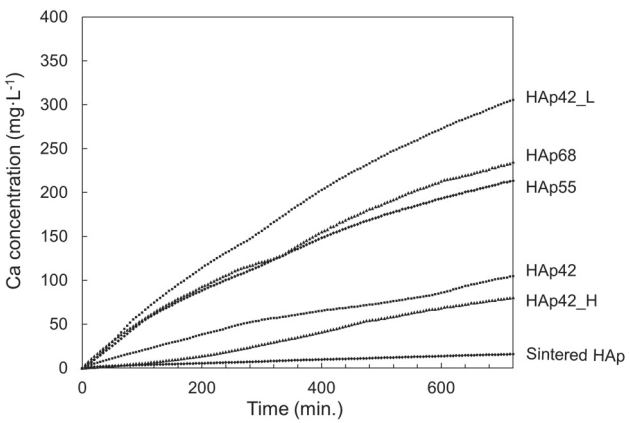

Fig. 5 Change in the elution of Ca ions from HAp blocks over time.

adhered onto the HAp blocks after incubation for 6 h. A comparison of the initial cell attachment among three samples with constant crystallite size and different porosities (HAp68, HAp55, and HAp42) indicated that there was no substantial difference between the three, although there were some statistically significant differences (HAp68>HAp42, HAp55>HAp42). We then compared the initial cell attachment of three different crystallite size samples at constant porosity (HAp42_L, HAp42, and HAp42_H) and found no significant difference between the three.

Figure 5 shows the change in the elution of Ca ions from the HAp blocks over time. The HAp block with the highest rate of Ca leaching was HAp42_L whereas the HAp block with the lowest rate was sintered HAp. Comparing the quantity of Ca ions eluted from the three HAp blocks with constant crystallite size and different porosities (HAp68, HAp55, and HAp42), the quantity of Ca ions eluted increased with increasing porosity (HAp68>HAp55>HAp42). When comparing the Ca ion release from three HAp blocks with different crystallite sizes at constant porosity (HAp42_L, HAp42, and HAp42_H), the Ca ion release increased as the crystallinity decreased (HAp42_L>HAp42>HAp42_H). The rate of Ca leaching from the HAp blocks increased with increasing SSA among all the HAp blocks.

DISCUSSION

Preparation of HAp blocks

We prepared HAp blocks through the setting reaction of calcium phosphate cement (HAp68, HAp55, HAp42, HAp42_L) and by general sintering (HAp42_H and sintered HAp). For the setting reaction of calcium phosphate cement, we prepared HAp blocks by the following chemical reactions [Eqs. 2 to 4][21].

Dissolution:

$$Ca_4(PO_4)_2O\ [TTCP]+H_2O \rightarrow 4Ca^{2+}+2PO_4^{3-}+2OH^- \quad [2]$$

$$CaHPO_4\ [DCPA] \rightarrow Ca^{2+}+H^++PO_4^{3-} \quad [3]$$

Precipitation:

$$2Ca_4(PO_4)_2O+2CaHPO_4 \rightarrow 10Ca^{2+}+6PO_4^{3-}+2OH^- \rightarrow Ca_{10}(PO_4)_6(OH)_2 \quad [4]$$

In this method, an aqueous solution containing phosphate ions is usually used to facilitate the phase conversion to HAp[21]. However, we used DI water because we intended to prepare HAp blocks with constant chemical composition. Because the use of DI water prevents the phase conversion to HAp compared with phosphate salt solution, we investigated the possibility of increasing the reactivity of the raw powders of TTCP. In particular, we examined the milling conditions of TTCP powder for the synthesis, referring to previous reports[25,26]. In addition, we determined a temperature for curing the set cement to establish the phase transformation to HAp. If the HAp that forms on the surface of the set cement in the initial stages of the reaction prevents further reactions inside the set cement, it will be difficult to achieve a phase transition of the entire set cement to HAp. Therefore, we set the curing temperature at 37°C in the first stage and then at 80°C in the second stage. We obtained single-phase HAp by using pulverized TTCP and two different temperatures for curing the set cement (Fig. 1).

To investigate the effect of the porosity and crystallinity of the HAp blocks, it was necessary to prepare a HAp block with a single HAp crystalline phase (Fig. 1). As for the contamination of carbonate ion into HAp blocks, it is reduced to the extent that it cannot be confirmed by Fourier transform infrared spectroscopy (data not shown). To investigate the effect of the porosity of the HAp blocks, we fabricated HAp blocks with almost the same crystallite size but different porosities (HAp68, HAp55, and HAp42). This study has shown that porosity can be controlled by the quantity of DI water used to make the cement slurry and the pressure applied to the cement slurry (Tables 1 and 2). Furthermore, to investigate the effect of the crystallinity of the HAp blocks, we fabricated HAp blocks with

almost the same porosities but different crystallite size (HAp42, HAp42_L, and HAp42_H). The crystalline size could be regulated by post-heat treatment temperature. The porosity could be regulated by the pressure loading on the cement slurry and the compacts. The pressure loading on the cement slurry and the compacts, and the post-heat treatment temperature, affected not only the porosity but also the SSA.

Protein adsorption and initial cell attachment of HAp blocks

When bone grafts are implanted *in vivo*, the first step is the adsorption of proteins in the body fluids onto the surface of the material[27]. Similarly, in our *in vitro* cell culture experiment, the adsorption of proteins from the culture medium to the HAp block surface is expected to occur before cell adhesion. Therefore, in this study, we first compared the protein adsorption behavior of the HAp block surface in the medium used for cell culture (Fig. 3). The reason for the increase in protein adsorption with increasing porosity (HAp68>HAp55>HAp42) is probably due to the increase in porosity, which increases the surface area available for protein adsorption. In the comparison between HAp68 and HAp42_L, the quantity of protein adsorbed by HAp42_L, which exhibited a large SSA, was significantly lower than that of HAp68, which exhibited a small SSA (Table 2 and Fig. 3); thus, a large SSA does not necessarily indicate that a large quantity of protein is adsorbed. In any case, this study revealed that the setting reaction of calcium phosphate cement can be used to fabricate HAp blocks, which can introduce nano- to submicron-sized pore structures by increasing the water-mixing ratio, thereby increasing the number of sites available for protein adsorption. The quantity of protein adsorption to the HAp blocks group prepared through the setting reaction of calcium phosphate cement (HAp68, HAp55, HAp42, and HAp42_L) was higher than that of HAp blocks group prepared by general sintering (HAp42_H and sintered HAp), suggesting that the nano- to submicron-sized pores that were present in HAp68, HAp55, HAp42, and HAp42_L (Fig. 2) may contribute to increase the effective surface area for protein adsorption.

Next, we considered the initial cell adhesion properties of the HAp block surface. Although there was a sample (HAp42_L) that exhibited significantly lower cell adhesion than the HAp68, HAp55 and control, the difference was small and they all exhibited good initial cell adhesion (Fig.4); suggesting that even the sintered HAp, which exhibited extremely low protein adsorption, is capable of adsorbing sufficient protein for MC3T3E1 cell adhesion, similarly to the other HAp blocks and control.

In vitro dissolution rate of HAp blocks

Dissolution tests of HAp blocks in an environment that mimics an osteoclast-created Howship's lacuna indicated that increasing the porosity and SSA had a significant effect on the dissolution rate of the HAp blocks. HAp blocks fabricated through the setting reaction of calcium phosphate cement introduced nano- to submicron-sized pores into the structure (Fig. 2). Weakly acidic liquids can penetrate into these pores and the increased contact area with the liquid improves its solubility. During the cell culture experiments, HAp68 and HAp55 exhibited substantial coloration from the cell culture medium; however, this was due to the introduction of a culture medium into the pore structure, and it was clear from these results that the pores were permeable to liquid. HAp42_L, which is the least crystalline, exhibited the highest solubility; but we hypothesize that the increase in SSA (due to the lower crystallinity) is directly responsible for the solubility. We observed formation of tiny air bubbles when we dipped HAp42_L into liquid. This is evidence of the uptake of liquid into the pores. In any case, this study has revealed that HAp blocks prepared through the setting reaction of calcium phosphate cement are effective for fabricating bioresorbable HAp bone grafts.

CONCLUSION

Fabrication of HAp blocks using the setting reaction of calcium phosphate cement enabled introduction of nano- to submicron-sized pores into the structure, which had little effect on the initial adhesion of MC3T3E1 cells, but it may contribute to the solubility in the osteoclast-producing environment of Howship's lacuna.

ACKNOWLEDGMENTS

This research was supported by a Grant-in-Aid for Scientific Research (B) (grant number 18H02987) from the Japanese Society for Promotion of Science and Research. We thank Edanz (https://jp.edanz.com/ac) for editing a draft of this manuscript.

REFERENCES

1) Aoki H. In: Aoki H., editor. Medical applications of hydroxyapatite. Tokyo, St Louis: Ishiyaku EuroAmerica, Inc.; 1994.
2) Bucholz RW, Carlton A, Holmes RE. Hydroxyapatite and tricalcium phosphate bone graft substitutes. Orthop Clin North Am 1987; 18: 323-334.
3) Ayers RA, Simske SJ, Nunes CR, Wolford LM. Long-term bone ingrowth and residual microhardness of porous block hydroxyapatite implants in humans. J Oral Maxillofac Surg 1998; 56: 1297-1301.
4) Waite PD, Morawetz RB, Zeiger HE, Pincock JL. Reconstruction of cranial defects with porous hydroxylapatite blocks. Neurosurgery 1989; 25: 214-217.
5) Bucholz RW, Carlton A, Holmes R. Interporous hydroxyapatite as a bone graft substitute in tibial plateau fractures. Clin Orthop 1988; 240: 53-62.
6) Yoshikawa H, Myoui A. Bone tissue engineering with porous hydroxyapatite ceramics. J Artif Organs 2005; 8: 131-136.
7) Teraoka K, Yokogawa Y, Kameyama T. Construction of an interconnected pore network using hydroxyapatite beads. Proceedings of 16th International Symposium on Ceramics in Medicine; 2003 Nov 6-9; Porto, Portugal. Trans Tech: Zurich, Switzerland; 2004. p. 257-259.
8) Karageorgiou V, Kaplan D. Porosity of 3D biomaterial

scaffolds and osteogenesis. Biomaterials 2005; 26: 5474-5491.
9) Zhang HG, Zhu Q. Preparation of porous hydroxyapatite with interconnected pore architecture. J Mater Sci Mater Med 2007; 18: 1825-1829.
10) Lee EJ, Koh YH, Yoon BH, Kim HE, Kim HW. Highly porous hydroxyapatite bioceramics with interconnected pore channels using camphene-based freeze casting. Mater Lett 2007; 61: 2270-2273.
11) Zhao K, Tang YF, Qin YS, Luo DF. Polymer template fabrication of porous hydroxyapatite scaffolds with interconnected spherical pores. J Euro Ceram Soc 2011; 31: 225-229.
12) Tang Y, Miao Q, Zhao K, Zhu M, Wu Z. Random stacking template of polymer spheres and water soluble particles to fabricate porous hydroxyapatite with interconnected pores. Ceram Int 2014; 40: 6631-6638.
13) Cho YS, Lee JS, Hong MW, Lee SH, Kim YY, Cho YS. Comparative assessment of the ability of dual-pore structure and hydroxyapatite to enhance the proliferation of osteoblast-like cells in well-interconnected scaffolds. Int J Precis Eng Manuf 2018; 19: 605-612.
14) Nassif N, Gobeaux F, Seto J, Belamie E, Davidson P, Panine P, *et al.* Self-assembled collagen–apatite matrix with bone-like hierarchy. Chem Mater 2010; 22: 3307-3309.
15) Olszta MJ, Douglas EP, Gower LB. Scanning electron microscopic analysis of the mineralization of type I collagen via a polymer-induced liquid-precursor (PILP) process. Calcif Tissue Int 2003; 72: 583-591.
16) Sang-Soo J, Thula TT, Gower LB. Development of bone-like composites via the polymer-induced liquid-precursor (PILP) process. Part 1: influence of polymer molecular weight. Acta Biomater 2010; 6: 3676-3686.
17) Wahl DA, Czernuszka JT. Collagen-hydroxyapatite composites for hard tissue repair. Eur Cell Mater 2006; 11: 43-56.
18) Parikh SN. Bone graft substitutes: past, present, future. J Postgrad Med 2002; 48: 142-148.
19) Kikuchi M, Itoh S, Ichinose S, Shinomiya K, Tanaka J. Self-organization mechanism in a bone-like hydroxyapatite/collagen nanocomposite synthesized *in vitro* and its biological reaction in vivo. Biomaterials 2001; 22: 1705-1711.
20) Kikuchi M. Developments of calcium phosphate-based bone regenerating materials utilizing interfacial interactions between inorganic-organic substances. J Ceram Soc Japan 2020; 128: 547-554.
21) Brown WE, Chow LC. A new calcium phosphate, water-setting cement. In: Brown PW, editor Cement research progress. Waterville, MA, USA: American Ceramics Society; 1986. p. 351-379.
22) Suresh S. Theoretical studies of solid state dielectric parameters of hydroxyapatite. Mater Phys Mech 2012; 14: 145-151.
23) Japanese Standards Association. JIS T 0330-3:2012 Bioceramics—Part 3: Testing method of measuring dissolution rate of calcium phosphate ceramics. Tokyo, Japan; 2012.
24) Ito A, Sogo Y, Yamazaki A, Aizawa M, Osaka A, Hayakawa S, *et al.* Interlaboratory studies on *in vitro* test methods for estimating *in vivo* resorption of calcium phosphate ceramics. Acta Biomater 2015; 25: 347-355.
25) Gbureck U, Barralet JE, Hofmann M, Thull R. Mechanical activation of tetracalcium phosphate. J Am Ceram Soc 2004; 87: 311-313.
26) Romeo HE, Fanovich MA. Synthesis of tetracalcium phosphate from mechanochemically activated reactants and assessment as a component of bone cements. J Mater Sci Mater Med 2008; 19: 2751-2760.
27) Wilson CJ, Clegg RE, Leavesley DI, Pearcy MJ. Mediation of biomaterial-cell interactions by adsorbed proteins: A review. Tissue Eng 2005; 11: 1-18.